

---

This is an electronic reprint of the original article.  
This reprint may differ from the original in pagination and typographic detail.

Anttu, Nicklas; Mäntynen, Henrik; Sorokina, Anastasiia; Kivisaari, Pyry; Sadi, Toufik; Lipsanen, Harri

## Geometry Tailoring of Emission from Semiconductor Nanowires and Nanocones

*Published in:*  
Photonics

*DOI:*  
[10.3390/photonics7020023](https://doi.org/10.3390/photonics7020023)

Published: 01/06/2020

*Document Version*  
Publisher's PDF, also known as Version of record

*Published under the following license:*  
CC BY

*Please cite the original version:*  
Anttu, N., Mäntynen, H., Sorokina, A., Kivisaari, P., Sadi, T., & Lipsanen, H. (2020). Geometry Tailoring of Emission from Semiconductor Nanowires and Nanocones. *Photonics*, 7(2), Article 23.  
<https://doi.org/10.3390/photonics7020023>

---

This material is protected by copyright and other intellectual property rights, and duplication or sale of all or part of any of the repository collections is not permitted, except that material may be duplicated by you for your research use or educational purposes in electronic or print form. You must obtain permission for any other use. Electronic or print copies may not be offered, whether for sale or otherwise to anyone who is not an authorised user.

Article

# Geometry Tailoring of Emission from Semiconductor Nanowires and Nanocones

Nicklas Anttu <sup>1,\*</sup>, Henrik Mäntynen <sup>1</sup>, Anastasiia Sorokina <sup>1</sup>, Pyry Kivisaari <sup>2</sup>, Toufik Sadi <sup>2</sup> and Harri Lipsanen <sup>1</sup>

<sup>1</sup> Department of Electronics and Nanoengineering, Aalto University, P.O. Box 13500, FI-00076 Aalto, Finland; henrik.mantynen@aalto.fi (H.M.); anastasiia.sorokina@aalto.fi (A.S.); harri.lipsanen@aalto.fi (H.L.)

<sup>2</sup> Engineered Nanosystems Group, Aalto University, P.O. Box 13500, FI-00076, Aalto, Finland; pyry.kivisaari@aalto.fi (P.K.); toufik.sadi@aalto.fi (T.S.)

\* Correspondence: nicklas.anttu@aalto.fi

Received: 24 February 2020; Accepted: 24 March 2020; Published: 26 March 2020

**Abstract:** Semiconductor nanowires are of interest as light emitters in applications such as light-emitting diodes and single-photon sources. Due to the three-dimensional geometry in combination with a size comparable to the wavelength of the emitted light, nanowires have shown strong scattering effects for the emitted light. Here, we demonstrate with electromagnetic modeling that the emission properties of nanowires/nanocones show a complicated dependence on the geometry of the nanowire/nanocone, the shape and position of the emitter region, and the polarization of the emitter. We show that with proper design, the extraction efficiency can close in on 80% for as-grown single nanowires/nanocones. Importantly, we demonstrate how the internal quantum efficiency of the emitter plays a large role in the design process. A considerably different geometry design approach should be undertaken at low and high internal quantum efficiency. Due to the complicated design optimization, we strongly recommend the use of electromagnetic modeling of the emission to give guidance for suitable designs before starting the fabrication and processing of nanowire/nanocone-based light emitters.

**Keywords:** semiconductor nanowire; directional emission; Purcell factor; internal quantum efficiency

---

## 1. Introduction

Semiconductor nanowires are of interest as light emitters in applications such as light-emitting diodes (LEDs), single-photon sources, and lasers [1–10]. In bottom-up fabricated nanowires, thanks to strain relaxation in the radial direction, it is possible to use combinations of semiconductor materials that are prohibitive in conventional thin-film devices due to lattice mismatch [11,12].

In addition to the materials science aspects, nanowires show novel optical behavior compared to planar thin-film devices. Due to the three-dimensional geometry in combination with size comparable to the wavelength of the emitted light, nanowires show a possibility for strong scattering effects for the emitted light [13–18]. Especially the diameter-to-wavelength ratio affects the emission properties strongly [7,14,19,20]. In addition to affecting the extraction of light and the emission directionality [14,17,18], the diameter modifies strongly the spontaneous emission rate through the Purcell factor [20,21].

However, the extraction of light from an as-grown nanowire on top of a substrate has not been considered in detail when varying the shape of the emitter region, the position of the emitter region, and the polarization of the emitter. Here, we study modeled emission from single nanowires and nanocones of varying diameter. We consider three cases for the emitter region: (i) emission from the

full nanowire/nanocone volume, (ii) emission from a 10 nm thick axial segment that spans the cross-section of the nanowire/nanocone, and (iii) an emitter located at the axis of the nanowire/nanocone. Furthermore, we consider (i) an unpolarized emitter, (ii) an emitter polarized in parallel to the nanowire/nanocone axis, and (iii) an emitter polarized perpendicularly to the axis. We show that with this combined design freedom, we can reach an extraction efficiency closing in on 80% for as-grown nanowires/nanocones.

We study the effect of the internal quantum efficiency (IQE) of the emitter on the design process. At low IQE, we should optimize the product of the extraction efficiency and the Purcell factor, whereas at high IQE, we should optimize solely the extraction efficiency. Since the extraction efficiency and the Purcell factor can show very different types of dependence on the design parameters, the optimum design for the nanowire/nanocone light emitter can be strongly dependent on the IQE.

In general, the emission properties show a complicated dependence on the geometry of the nanowire/nanocone, the shape and position of the emitter region, the polarization of the emitter, and the IQE. Due to this complicated dependence, we believe that electromagnetic modeling is valuable for giving guidance for suitable designs before starting the fabrication and processing of nanowire/nanocone light emitters.

## 2. Materials and Methods

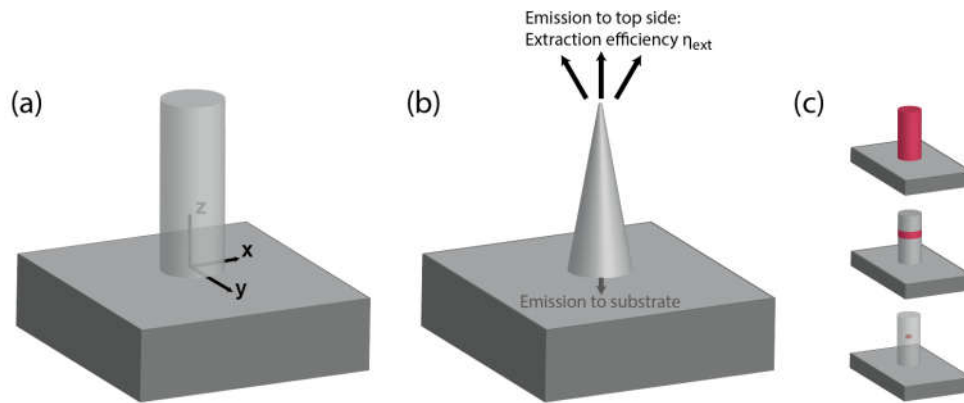


**Figure 1.** (a) Semiconductor nanowire of diameter  $D$  and length  $L = 1000$  nm on top of a semi-infinite semiconductor substrate. (b) Semiconductor nanocone of base diameter  $D$  and length  $L = 1000$  nm on top of a semi-infinite semiconductor substrate. (c) The three configurations we consider for the emission region, which is marked in red: (top) emission from the whole nanowire/nanocone, (middle) emission from a 10 nm thick axial segment throughout the whole cross-section of the nanowire/nanocone, and (bottom) an emitter located at the axis of the nanowire/nanocone. The coordinate system is chosen such that  $z = 0$  is at the top of the substrate,  $z = L$  is at the top of the nanowire/nanocone, and the nanowire/nanocone axis is at  $x = y = 0$  (see (a) for the coordinate axes).

We consider emission from a single nanowire/nanocone on top of a semi-infinite substrate (see Figure 1a,b for schematics). Our focus is toward nanowire/nanocone LED applications, where we are interested in the overall emission to the top side. Thus, in our analysis of the results, we do not analyze in detail through which optical modes of the nanowire/nanocone the emission occurs, in strong contrast to nanowire single-photon applications where emission predominantly through a single, well-defined optical mode in the nanowire is desirable [1].

The nanowire/nanocone is of a (base) diameter  $D$  and length  $L = 1000$  nm. We consider a dipole emitter, and the emission is modeled by solving Maxwell’s equations. The diffraction of light by the nanowire/nanocone is taken into account through the geometry and the refractive index of the nanowire/nanocone. Technically, we model the emission with the Lorentz reciprocity where the response of an incident plane wave at the location of the dipole emitter is recorded [17,18,22]. From the electric field induced by the plane wave at the position of the dipole emitter, we obtain through

the Lorentz reciprocity the emission intensity of the plane wave radiated by the dipole in the reciprocal direction of the incident plane wave that was used in the modeling [17,18,22]. For each emission angle considered, we perform separate modeling for each of the two orthogonal polarization states of the emitted light (which is not to be confused with the polarization/orientation of the dipole itself). The modeling is performed with Comsol Multiphysics, similarly as described by us in Appendix D in Ref. [17]. Here, in addition, we resolve the  $x$ -,  $y$ -, and  $z$ -components of the electric field induced by the incident plane wave at the position of the dipole, which allows us to compare the emission from  $x$ -,  $y$ -, and  $z$ -oriented dipoles. Through modeling, we calculate the response of a parallel-to-axis  $z$ -oriented dipole and a perpendicular-to-axis oriented dipole, for which we averaged the results for an  $x$ - and an  $y$ -oriented dipole.

We model a nanowire/nanocone of refractive index  $n_{\text{semi}} = 3.5$ , which is a typical value for many III–V semiconductors, such as InP, at their bandgap wavelength. The nanowire is placed on top of a semiconductor substrate, also of  $n_{\text{semi}}$ . Note that since the nanowire is on top of the high-refractive index substrate, all the emitted light couples either to the air top side or into the substrate, since no in-plane guided modes are present at the air/substrate interface [17]. Hence, our modeling with the Lorentz reciprocity takes into account all available emission pathways. In this study, we focus on an emission wavelength of  $\lambda = 920$  nm, to correspond to emission from InP at room temperature. Note that our results remain invariant to a scaling of all geometrical dimensions with a constant factor  $a$ , if the wavelength is scaled with the same factor  $a$  (as long as the refractive index does not show noticeable wavelength dependence).

We consider three cases for the emitter region: (i) incoherent dipoles distributed in the whole nanowire/nanocone volume (top schematic of Figure 1c), (ii) incoherent dipoles distributed in a 10 nm thick segment that spans the whole  $x$ - $y$  cross-section of the nanowire/nanocone (middle schematic of Figure 1c), and (iii) a dipole located at the axis of the nanowire/nanocone (bottom schematic of Figure 1c). We consider incoherent dipoles in order to focus on spontaneous emission from an extended emitter region, and we average the response of dipoles distributed throughout the emitter region [17]. Due to the high rotational symmetry in all these three cases, in combination with the dipole orientations considered (either  $z$ -oriented dipole, which we denote in shorthand as  $p_z$ , or averaging over the  $x$  and  $y$  oriented dipole, which we denote in shorthand as  $p_x/p_y$  averaged), we model the emission only for varying polar angle,  $\theta$ , at a fixed azimuthal angle  $\varphi$ . For the emitter on the nanowire axis, case (iii), the  $z$ -oriented dipole does not show  $\varphi$  dependence in the emission, and the averaging of  $x$ - and  $y$ -oriented dipoles for the perpendicular-to-axis dipole gives a  $\varphi$ -independent emission. For the extended emitter regions, cases (i) and (ii), due to the rotational symmetry of the problem, the  $\varphi$  dependence of the emission at a given off-axis position is implicitly included through the averaging over the dipole position (which includes a  $\varphi$  integration for the dipole position).

We can calculate the emitted power to the air top side,  $P_{\text{top}}$ , and into the substrate,  $P_{\text{bot}}$ , by integrating the angle-dependent emission over the emission angles into the respective half-spaces [17,18]. The total emitted intensity is given by  $P_{\text{tot}} = P_{\text{top}} + P_{\text{bot}}$ , and the extraction efficiency to the top side is given by  $\eta_{\text{ext}} = P_{\text{top}} / P_{\text{tot}}$ . For the Purcell factor,  $C_{\text{Purcell}}$ , we calculate first the emitted intensity,  $P_{\text{semi}}$  of a dipole into a homogeneous surrounding of  $n_{\text{semi}}$ . Then,  $C_{\text{Purcell}} = P_{\text{tot}} / P_{\text{semi}}$ . We modeled the emission with a step of  $1^\circ$  in  $\theta$ , from which we calculated  $\eta_{\text{ext}}$  and  $C_{\text{Purcell}}$ . To ascertain that this stepping was fine enough to avoid numerical artefacts, we compared those values with the values for  $\eta_{\text{ext}}$  and  $C_{\text{Purcell}}$  calculated from an integration with a coarser stepping of  $2^\circ$  in  $\theta$ .

### 3. Results

#### 3.1. Unpolarized Dipole

In a III–V semiconductor of the zinc-blende crystal phase, which is the crystal phase found for non-nitride bulk III–V semiconductors, the dipole emitter does not have a preferred direction. In that case, to consider an unpolarized dipole, we average the results for an  $x$ -, an  $y$ -, and a  $z$ -oriented dipole at each considered position. We start by studying emission from the whole nanowire/nanocone volume (Figure 2).

For nanowires, we reach an extraction efficiency of 53% at a diameter of 180 nm (Figure 2a). At this diameter, we expect enhanced coupling to the fundamental HE<sub>11</sub> guided mode [23]. Note that if the wavelength or refractive index of the nanowire are varied, the diameter at which the peak occurs is expected to shift in a manner such that  $n_{\text{semi}}D/\lambda$  stays constant [24]. For the HE<sub>11</sub> mode, we expect that the emission peaks in the direction parallel to the nanowire axis [16]. When studying the directionality of the emission, we indeed see a peak in the emission at  $\theta = 0$  at  $D = 180$  nm (inset in Figure 2a). For the three other diameters in that inset, that is, the smallest  $D = 100$  nm considered in this study,  $D = 310$  nm where the next peak in  $\eta_{\text{ext}}$  occurs, and the largest  $D = 400$  nm considered, we find a more complicated directionality pattern.

For nanocones, we do not reach above 30% in extraction efficiency (Figure 2b). Interestingly, for the nanocones,  $\eta_{\text{ext}}$  shows much less dependence with diameter than for the nanowires in Figure 2a. For the nanocones, the emission peaks at  $\theta = 0$  for all the four  $D = 100, 150, 250,$  and  $400$  nm considered in the inset of Figure 2b (here  $D = 150$  and  $250$  nm were chosen, since  $C_{\text{Purcell}}$  shows, respectively, a dip and a peak there). Thus, there appears to be noticeable differences in the emission properties between a nanowire and a nanocone.

For both nanowires and nanocones, the extraction efficiency tends to decrease with increasing diameter. The Purcell factor, on the other hand, tends to increase with increasing diameter (red curves in Figure 2a,2b). However, note that there are noticeable peaks and dips in both  $C_{\text{Purcell}}$  and  $\eta_{\text{ext}}$ . For example, for nanowires, the peaks coincide at  $D = 310$  nm. Thus, it is possible to find designs where both  $C_{\text{Purcell}}$  and  $\eta_{\text{ext}}$  are simultaneously high.

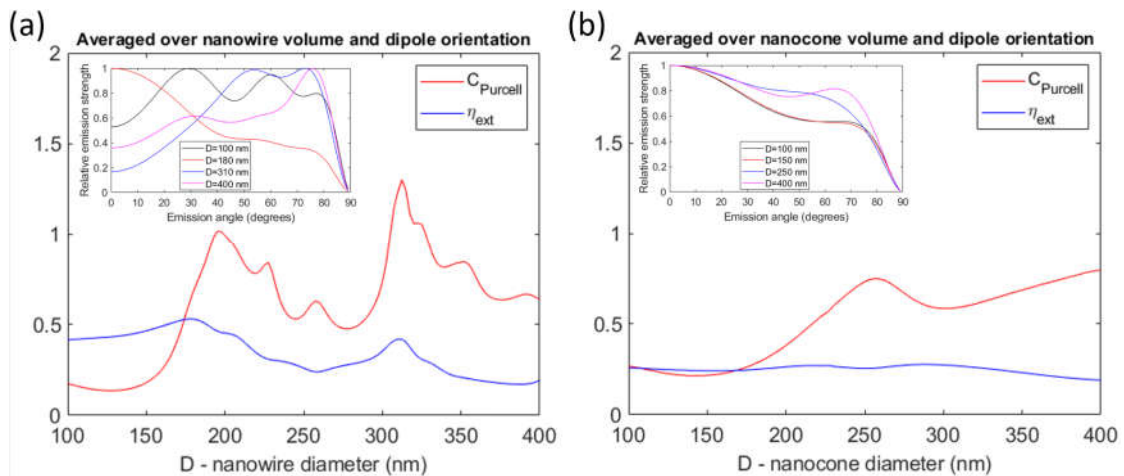


**Figure 2.** Purcell factor,  $C_{\text{Purcell}}$ , and extraction efficiency,  $\eta_{\text{ext}}$ , when averaging over dipoles distributed throughout the full volume of the (a) nanowire and (b) nanocone. Here, we consider an unpolarized dipole. That is, we average the results from  $x$ -,  $y$ -, and  $z$ -oriented dipoles for each position. The insets show, for selected  $D$ , the normalized relative emission strength to the top side as a function of polar angle  $\theta$  with  $\theta = 0$  corresponding to emission into a direction parallel to the nanowire/nanocone axis (note that to study the relative emitted power into polar angle  $\theta$  integrated over azimuth angle  $\varphi$ , these values should be multiplied by  $\sin(\theta)$ ).

### 3.1.1. Dependence on Axial Position

Next, we consider emission from a 10 nm thick axial segment, with averaging over the  $x$ - $y$  cross-section for the dipole position (Figure 3) (note that the color scales are kept the same through Figures 3–7 for easy comparison). For example, this case could correspond to emission from a well-defined depletion region in an axial p–n junction.

Here, we find a complicated dependence with the diameter of the nanowire/nanocone and the axial position of the emitter region. In general, we find more structure in the patterns for the nanowires than for the nanocones. One explanation to a stronger dependence of the axial position of the emitter could be the stronger reflection at the nanowire–air top interface compared to at the

nanocone–air top interface [1,7,8]. In nanowires, a Fabry-Perot standing wave pattern from a given mode can occur in the axial direction due to reflection at both the top and the bottom interface. Depending on how the emitter is placed relative to the nodes of that standing wave pattern, enhanced or decreased coupling of emission to the mode could occur. In contrast, in nanocones, the lack of efficient back-reflection of a mode at the top interface is expected to lead to much weaker standing wave effects.

Another difference between a nanowire and a nanocone is that the nanowires support the same guided mode through the whole nanowire. In contrast, in the nanocones, each guided mode changes adiabatically with the axial position, since the effective diameter changes continuously from the top to the bottom of the cone. Such adiabatic change in a mode affects the coupling of the emitter to the modes, possibly explaining why much more noticeable dependence on diameter is found for the nanowire compared to the nanocone.

For  $D < 200$  nm, with appropriate placement of the emitter region along the axis of the nanowire/nanocone, we can reach above 60% extraction efficiency with the nanowires and above 50% extraction efficiency with the nanocones, which is an especially large increase for the nanocones that did not reach above 30% when considering emission from the full nanocone volume (Figure 2b).

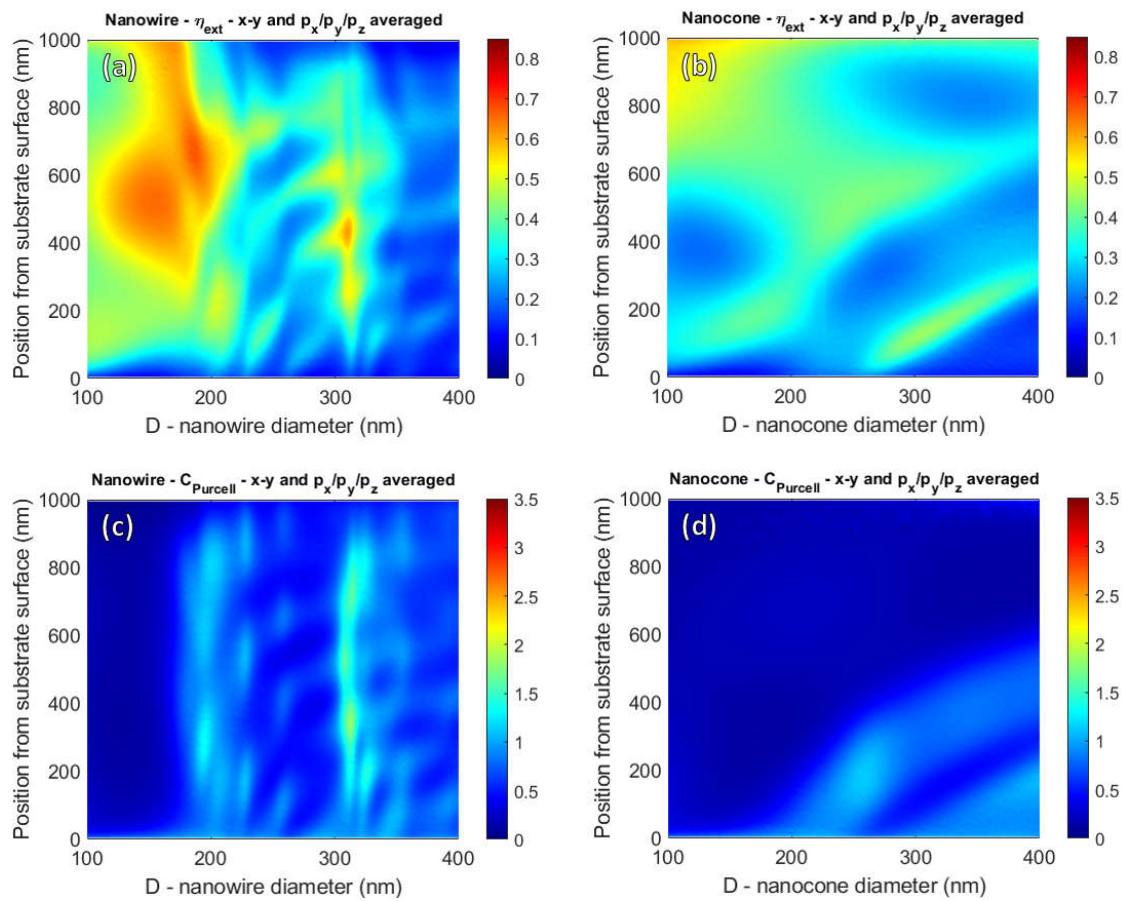


**Figure 3.** (a,b) Extraction efficiency,  $\eta_{ext}$ , and (c,d) Purcell factor,  $C_{Purcell}$ , for (a,c) a nanowire and (b,d) a nanocone. Here, we consider an emitter region that is 10 nm thick in the axial  $z$ -direction, and we average for dipoles distributed in that  $x$ - $y$  cross-section (as indicated in the figure titles by  $x$ - $y$  averaged). Furthermore, we consider an unpolarized dipole. That is, we average the results from  $x$ -,  $y$ -, and  $z$ -oriented dipoles for each position (as indicated in the figure titles by  $p_x/p_y/p_z$  averaged).

### 3.1.2. Dipole at the Axis of Nanowire/Nanocone

Next, we move to consider an emitter located exactly at the axis of the nanowire/nanocone, which could correspond for example to emission from a quantum dot within the nanowire/nanocone

[1]. Here, for nanowires, we find much stronger oscillations with the diameter and axial position of the emitter (Figures 4a,c) compared to the case of the emitter region spanning the full cross-section at a given axial position (Figures 3a,c). Thus, different design recommendations can apply for the geometry of the nanowire and the placement of the emitter region, depending on whether the emitter region is confined to the vicinity of the nanowire axis or spans the full  $x$ - $y$  cross-section.

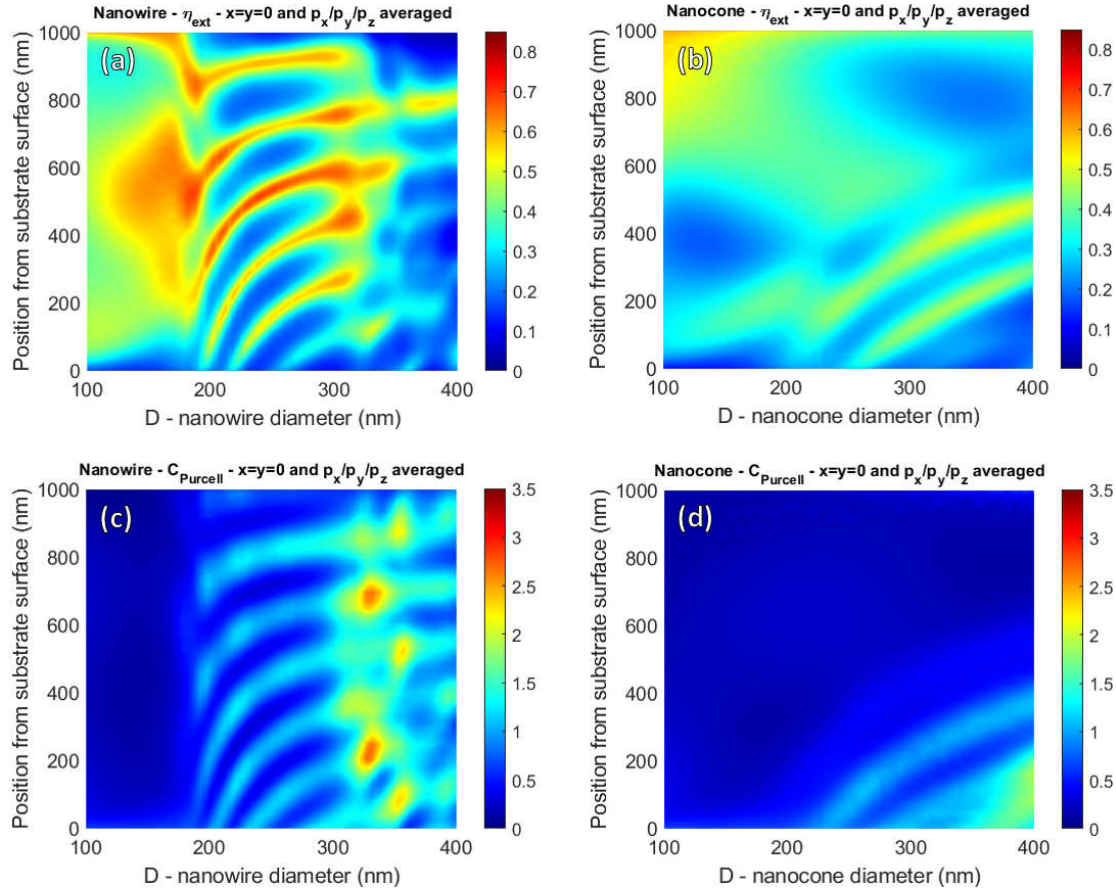


**Figure 4.** (a,b) Extraction efficiency,  $\eta_{\text{ext}}$ , and (c,d) Purcell factor,  $C_{\text{Purcell}}$ , for (a,c) a nanowire and (b,d) a nanocone. Here, we consider an emitter located at the axis of the nanowire/nanocone (as indicated in the figure titles by  $x=y=0$ ). Furthermore, we consider an unpolarized dipole. That is, we average the results from  $x$ -,  $y$ -, and  $z$ -oriented dipoles for each position (as indicated in the figure titles by  $p_x/p_y/p_z$  averaged).

Especially in the region  $200 < D < 300$  nm, we find well-defined fringes for the nanowire. We expect more well-defined enhanced or suppressed coupling to the standing wave pattern of a guided mode when the emitter is at a well-defined position in the  $x$ - $y$  cross-section. At  $D = 200$  nm, the peaks are separated by  $\Delta z_{\text{emitter}} \approx 262$  nm, and at  $D = 300$  nm, the peaks are separated by  $\Delta z_{\text{emitter}} \approx 165$  nm, where  $z_{\text{emitter}}$  is the position of the emitter from the substrate surface. The condition for such a standing wave is  $n_{\text{eff}}(2\pi/\lambda)2\Delta z_{\text{emitter}} = 2\pi$ , which gives  $n_{\text{eff}} = \lambda/(2\Delta z_{\text{emitter}})$ . Here,  $n_{\text{eff}}$  is the effective refractive index of the mode giving rise to the fringes. From the extracted  $\Delta z_{\text{emitter}}$  values, we obtain  $n_{\text{eff}} = 1.76$  at  $D = 200$  nm and  $n_{\text{eff}} = 2.79$  at  $D = 300$  nm. These values are in excellent agreement with the  $n_{\text{eff}} = 1.75$  and  $n_{\text{eff}} = 2.79$  that we obtain for the  $\text{HE}_{11}$  mode at  $D = 200$  and 300 nm by solving for the semi-analytical dispersion relation of the mode in the nanowire waveguide [23].

We reach a considerably higher maximum Purcell factor by confining the emitter to the axis: approximately 2.5 as the maximum Purcell factor for the nanowires (Figure 4c) and 1.8 for the nanocones (Figure 4d), compared to 1.6 for the nanowires in Figure 3b and 1.1 for the nanocones in

Figure 3d, where the emitter region extends throughout the  $x$ - $y$  cross-section. However, we do not reach considerably higher maximum extraction efficiency by confining the emitter to the axis.

### 3.2. Parallel-to-axis vs Perpendicular-to-axis Oriented Dipole

For example, if considering nanowires of the wurtzite crystal phase, the dipole emitter is  $z$ -oriented [25] (assuming that the crystallographic [1000] direction of the wurtzite phase is parallel to the nanowire/nanocone axis). In contrast, with quantum dots, the direction of the emitter is typically perpendicular to the axis of the nanowire/nanocone [26]. Therefore, we consider the effect of the orientation/polarization of the emitter. When comparing results for an  $x$ - $y$ -oriented dipole (Figure 5) with a  $z$ -oriented dipole (Figure 6), we find a rather different dependence on the diameter and  $z_{\text{emitter}}$ . Importantly, the optimum diameter and placement of the emitter region do not seem to coincide for the  $z$ -oriented and  $x$ - $y$ -oriented dipoles. Therefore, if we consider a  $z$ - or an  $x$ - $y$ -polarized emitter, we could expect higher maximum extraction efficiency and Purcell factor compared to the unpolarized emitter considered above (since for the unpolarized emitter, we average over the different orientations of the dipole emitter, for which the optimum designs do not coincide).

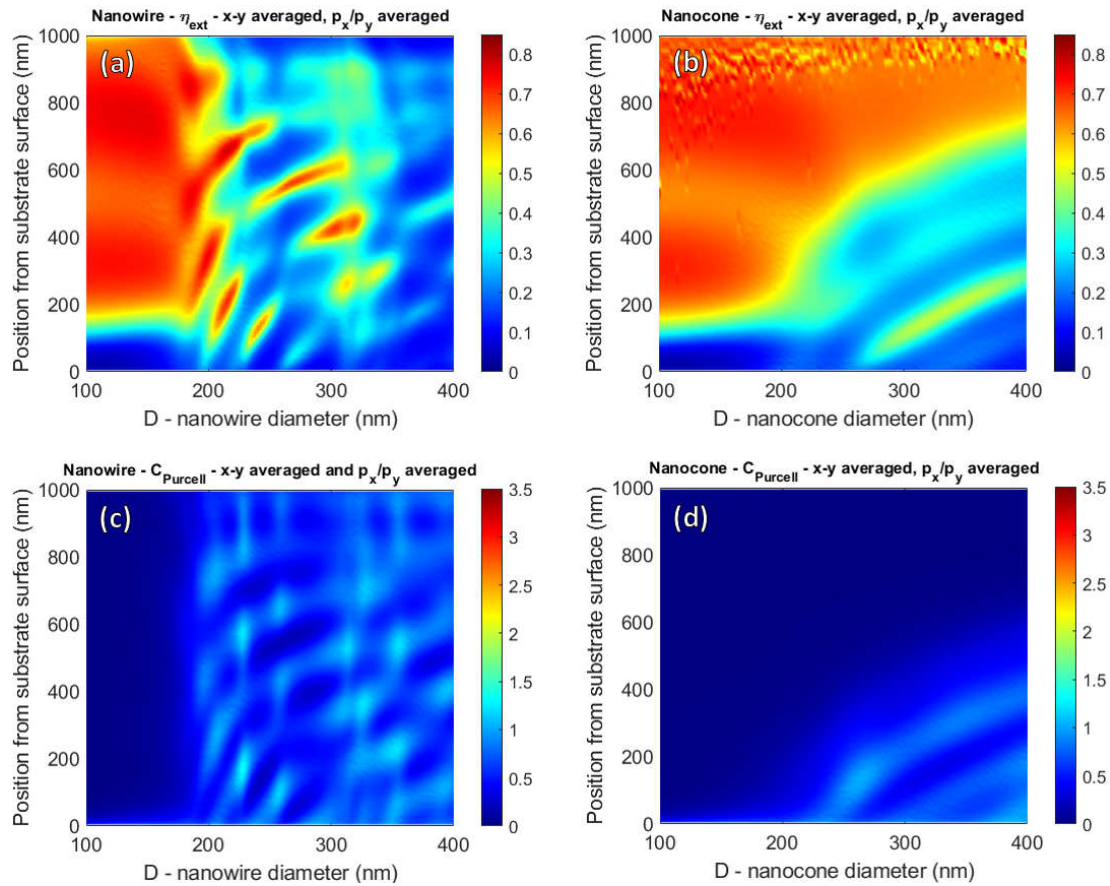


**Figure 5.** (a,b) Extraction efficiency,  $\eta_{\text{ext}}$ , and (c,d) Purcell factor,  $C_{\text{Purcell}}$ , for (a,c) a nanowire and (b,d) a nanocone. Here, we consider an emitter region that is 10 nm thick in the axial  $z$  direction, and we average for dipoles distributed in that  $x$ - $y$  cross-section (as indicated in the figure titles by  $x$ - $y$  averaged). Furthermore, we consider an in-plane oriented dipole. That is, we average the results from  $x$ - and  $y$ -oriented dipoles for each position (as indicated in the figure titles by  $p_x/p_y$  averaged).

For the  $x$ - $y$ -oriented dipole, we find for  $D < 200$  nm in both nanowires and nanocones an extraction efficiency above 70% (Figure 5a,b: Note that for  $z_{\text{emitter}} > 800$  nm in the nanocones,  $\eta_{\text{ext}}$  varies rapidly in the range from 0.55 to 0.8, and the origin of this intriguing behavior is left for future

studies). However, there, the Purcell factor is low (Figure 5c,d). Overall, with the  $x$ - $y$ -oriented dipole, we reach a maximum Purcell factor of approximately 1.2.

For the  $z$ -oriented dipole, we find a maximum extraction efficiency of 0.73 when  $D = 190$  nm and  $z_{\text{emitter}} = 670$  nm (Figure 6a). For the nanowires, the Purcell factor shows a peak value of 3.1 for  $D = 310$  nm and  $z_{\text{emitter}} = 290$  nm (Figure 6c). In the nanocone geometry, we reach a maximum extraction efficiency of 0.55 for  $D = 100$  nm and  $z_{\text{emitter}} = 990$  nm (Figure 6b), whereas the Purcell factor peaks at 2.2 at  $D = 260$  nm and  $z_{\text{emitter}} = 230$  nm (Figure 6d).

Here, we focused on an extended emitter region in the cross-section. When considering an emitter located at the axis (not shown), we did not find considerably higher peak values. However, we did find a noticeably different location of the peaks, similarly as for the unpolarized dipole when comparing the extended emitter in Figure 3 and the emitter located at the axis in Figure 4.

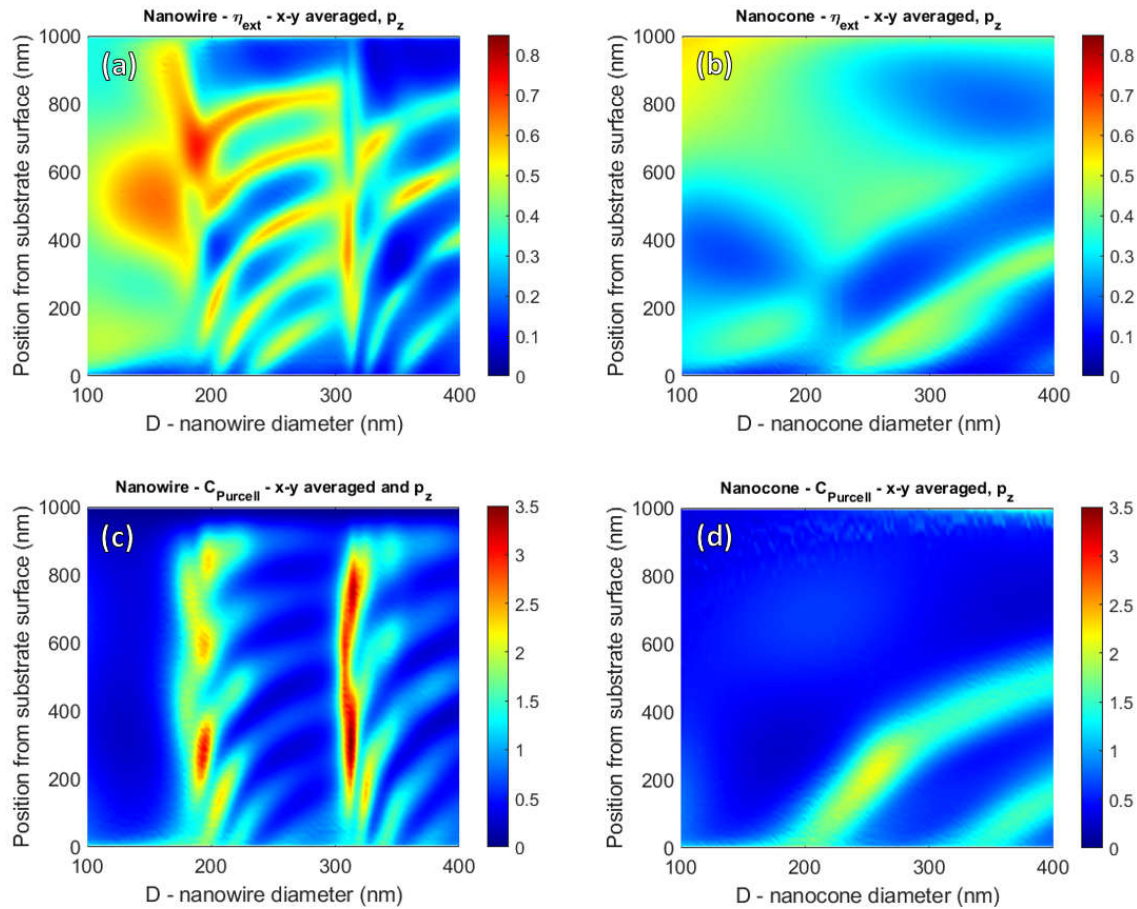


**Figure 6.** (a,b) Extraction efficiency,  $\eta_{\text{ext}}$ , and (c,d) Purcell factor,  $C_{\text{Purcell}}$ , for (a,c) a nanowire and (b,d) a nanocone. Here, we consider an emitter region that is 10 nm thick in the axial  $z$ -direction, and we average for dipoles distributed in that  $x$ - $y$  cross-section (as indicated in the figure titles by  $x$ - $y$  averaged). Furthermore, we consider a parallel-to-axis oriented dipole. That is, we model a  $z$ -oriented dipole for each position (as indicated in the figure titles by  $p_z$ ).

### 3.3. Optimized Design for Varying IQE

For the emitter in a homogeneous surrounding, we assume a radiative recombination rate  $\Gamma_{\text{rad},0}$  and a non-radiative recombination rate  $\Gamma_{\text{nr}}$  giving an internal quantum efficiency of  $\text{IQE}_0 = \Gamma_{\text{rad},0}/(\Gamma_{\text{rad},0} + \Gamma_{\text{nr}})$ . When the emitter is placed inside the nanowire/nanocone, the radiative recombination rate is modified by the Purcell factor:  $\Gamma_{\text{rad}} = C_{\text{Purcell}}\Gamma_{\text{rad},0}$ . If we assume that  $\Gamma_{\text{nr}}$  is not modified by the change in geometry, we obtain for the emitter in the nanowire/nanocone:  $\text{IQE} = \Gamma_{\text{rad}}/(\Gamma_{\text{rad}} + \Gamma_{\text{nr}})$ , which can be rewritten with the above definitions as  $\text{IQE} = C_{\text{Purcell}}\text{IQE}_0/$

$[C_{\text{Purcell}}IQE_0 + (1 - IQE_0)]$ . (Note that for emission from the full volume of an unpassivated nanowire/nanocone, the non-radiative recombination rate due to surface recombination is expected to vary with the diameter of the nanowire/nanocone [27]. In contrast, if it is the thickness of a passivation layer that is varied, we expect the assumption of a non-varying  $\Gamma_{\text{nr}}$  to be better motivated.) Finally, since we neglect parasitic absorption and re-absorption, the external quantum efficiency is given as

$$EQE = \eta_{\text{ext}}IQE = \frac{\eta_{\text{ext}}C_{\text{Purcell}}IQE_0}{C_{\text{Purcell}}IQE_0 + (1 - IQE_0)} \quad (1)$$

From the above definitions of EQE and IQE, we see that if the initial  $IQE_0$  is very high, that is very close to 100%,  $EQE \approx \eta_{\text{ext}}$ . Thus, the Purcell factor does not modify EQE, since  $IQE \approx 100\%$ . In that case, almost all recombination is radiative, and only the probability to extract those photons to the top side affects EQE (but note that the Purcell factor still modifies the output power at a given voltage in an LED [18]). In contrast, if the initial  $IQE_0$  is very low, that is close to zero,  $EQE \approx \eta_{\text{ext}}C_{\text{Purcell}}IQE_0$ . Thus, also here, the extraction efficiency is central for EQE, but now, in addition, also the Purcell factor modifies EQE linearly. Therefore, the metric that should be optimized depends on  $IQE_0$ . At high  $IQE_0$ , we should focus on optimizing just  $\eta_{\text{ext}}$  (see Figure 7a), whereas at low  $IQE_0$ , we should optimize  $\eta_{\text{ext}}C_{\text{Purcell}}$  (see Figure 7c). Therefore, for a given system, the  $IQE_0$  can affect strongly the way in which we should design the geometry and emitter location; see the difference between Figure 7a (high  $IQE_0$ ) and Figure 7c (low  $IQE_0$ ).

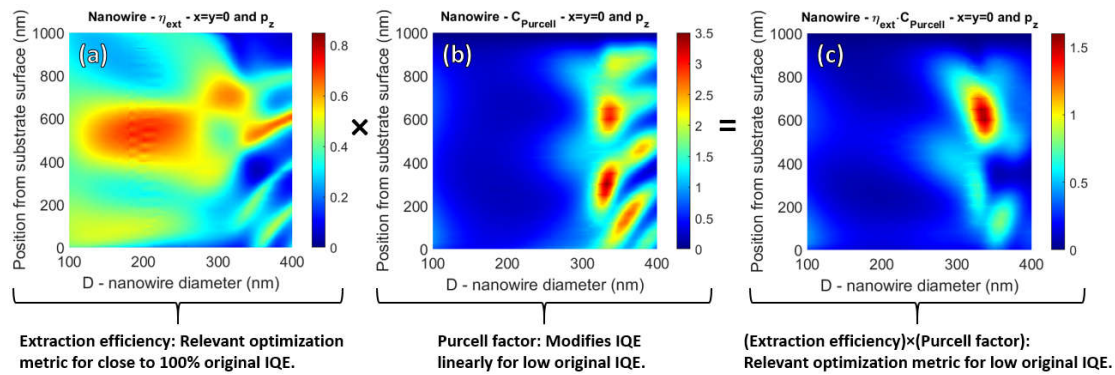


**Figure 7.** (a) Extraction efficiency,  $\eta_{\text{ext}}$ , (b) Purcell factor,  $C_{\text{Purcell}}$ , and (c)  $\eta_{\text{ext}}C_{\text{Purcell}}$  of a nanowire. Here, we consider an emitter located at the axis of the nanowire (as indicated in the figure titles by  $x = y = 0$ ). Furthermore, we consider a parallel-to-axis oriented dipole. That is, we model a z-oriented dipole for each position (as indicated in the figure titles by  $p_z$ ).

#### 4. Discussion

As shown above, the optimum design with regard to the diameter of the nanowire/nanocone depends on the polarization of the emitter, the extent and position of the emitter region, and even the IQE. For example, for the system in Figure 7, if we assume a high IQE, we could choose a design with  $D \approx 200$  nm and  $z_{\text{emitter}} \approx 500$  nm to optimize the extraction efficiency in Figure 7a. However, if the system had a low IQE, then, if instead of the  $D \approx 200$  nm and  $z_{\text{emitter}} \approx 500$  nm, we would choose  $D \approx 340$  nm and  $z_{\text{emitter}} \approx 600$  nm, we would reach a 10 times higher value for  $\eta_{\text{ext}}C_{\text{Purcell}}$  (Figure 7c), which is the relevant performance metric at low IQE. Thus, it can be of the highest importance to take the IQE into account in the design process.

We strongly recommend performing electromagnetic modeling of the emission before starting large-scale fabrication and the optimization of nanowire light emitters. Such modeling will (i) give direction for suitable design to aim for and (ii) give guidance on how sensitive the expected performance is to small variations from the optimum design. For example, to aim for the peak in extraction efficiency that occurs around  $D \approx 310$  nm and  $z_{\text{emitter}} \approx 400$  nm in Figure 6a is somewhat hazardous, since even just a 10 nm variation from the intended diameter could cause a 50% relative

drop in extraction efficiency. Instead, guided by modeling, the peak that occurs at  $D \approx 200$  nm and  $Z_{\text{emitter}} \approx 650$  nm in Figure 6a appears as a much more robust option against such small variations in diameter.

Inspired by the present study of the strong geometry tuneability of the emission from nanowires and nanocones, we believe that for example, the following directions are of interest for further research: (1) emission from radially configured emitter regions [3], (2) the effect of parasitic absorption in metallic or transparent conductive oxide contact layers [4,5], and (3) the effect of re-absorption and photon recycling in the active emitter region [28].

**Author Contributions:** Conceptualization, N.A., H.M., A.S., P.K., T.S. and H.L.; methodology, N.A., H.M., A.S., P.K., T.S.; validation; N.A. All authors have read and agreed to the published version of the manuscript.

**Funding:** This work is supported by the Academy of Finland [Grant No. 320167 (PREIN Flagship - Aalto University)].

**Acknowledgments:** We acknowledge the computational resources provided by the Aalto Science-IT project.

**Conflicts of Interest:** The authors declare no conflict of interest. The funders had no role in the design of the study; in the collection, analyses, or interpretation of data; in the writing of the manuscript, or in the decision to publish the results.

## References

- Mäntynen, H.; Anttu, N.; Sun, Z.; Lipsanen, H. Single-photon sources with quantum dots in III-V nanowires. *Nanophotonics* **2019**, *8*, 747–769.
- Monemar, B.; Ohlsson, B.J.; Gardner, N.F.; Samuelson, L. Nanowire-based visible light emitters, present status and outlook. *Semicond. Semimet.* **2016**, *94*, 227–271.
- Berg, A.; Yazdi, S.; Nowzari, A.; Storm, K.; Jain, V.; Vainorius, N.; Samuelson, L.; Wagner, J.B.; Borgström, M.T. Radial Nanowire Light-Emitting Diodes in the  $(\text{Al}_x\text{Ga}_{1-x})_y\text{In}_{1-y}\text{P}$  Material System. *Nano Lett.* **2016**, *16*, 656–662.
- Svensson, C.P.T.; Mårtensson, T.; Trägårdh, J.; Larsson, C.; Rask, M.; Hessman, D.; Samuelson, L.; Ohlsson, J. Monolithic GaAs/InGaP nanowire light emitting diodes on silicon. *Nanotechnology* **2008**, *19*, 305201.
- Motohisa, J.; Kohashi, Y.; Maeda, S. Far-field emission patterns of nanowire light-emitting diodes. *Nano Lett.* **2014**, *14*, 3653–3660.
- Guan, N.; Dai, X.; Julien, F.H.; Eymery, J.; Durant, C.; Tchernycheva, M. Nitride nanowires for light emitting diodes. In *Light-Emitting Diodes*; Ji, L., Chang, G.Q., Eds.; Springer: Berlin, Germany, 2019; pp. 425–484.
- Reimer, M.E.; Bulgarini, G.; Akopian, N.; Hocevar, M.; Bavinck, M.B.; Verheijen, M.A.; Bakkers, E.P.; Kouwenhoven, L.P.; Zwiller, V. Bright single-photon sources in bottom-up tailored nanowires. *Nat. Commun.* **2012**, *3*, 737.
- Claudon, J.; Bleuse, J.; Malik, N.S.; Bazin, M.; Jaffrennou, P.; Gregersen, N.; Sauvan, C.; Lalanne, P.; Gérard, J. A highly efficient single-photon source based on a quantum dot in a photonic nanowire. *Nat. Photonics* **2010**, *4*, 174–177.
- Xu, W.; Ren, F.; Jevtics, D.; Hurtado, A.; Li, L.; Gao, Q.; Ye, J.; Wang, F.; Guilhabert, B.; Fu, L. Vertically emitting indium phosphide nanowire lasers. *Nano Lett.* **2018**, *18*, 3414–3420.
- Chen, S.; Jansson, M.; Stehr, J.E.; Huang, Y.; Ishikawa, F.; Chen, W.M.; Buyanova, I.A. Dilute nitride nanowire lasers based on a GaAs/GaNAs core/shell structure. *Nano Lett.* **2017**, *17*, 1775–1781.
- Björk, M.; Ohlsson, B.; Sass, T.; Persson, A.; Thelander, C.; Magnusson, M.; Deppert, K.; Wallenberg, L.; Samuelson, L. One-dimensional steeplechase for electrons realized. *Nano Lett.* **2002**, *2*, 87–89.
- Gudiksen, M.S.; Lauhon, L.J.; Wang, J.; Smith, D.C.; Lieber, C.M. Growth of nanowire superlattice structures for nanoscale photonics and electronics. *Nature* **2002**, *415*, 617–620.
- Grzela, G.; Paniagua-Domínguez, R.; Barten, T.; Fontana, Y.; Sánchez-Gil, J.A.; Gómez Rivas, J. Nanowire antenna emission. *Nano Lett.* **2012**, *12*, 5481–5486.
- Paniagua-Domínguez, R.; Grzela, G.; Rivas, J.G.; Sánchez-Gil, J.A. Enhanced and directional emission of semiconductor nanowires tailored through leaky/guided modes. *Nanoscale* **2013**, *5*, 10582–10590.
- Grzela, G.; Paniagua-Domínguez, R.; Barten, T.; van Dam, D.; Sánchez-Gil, J.A.; Rivas, J.G. Nanowire antenna absorption probed with time-reversed Fourier microscopy. *Nano Lett.* **2014**, *14*, 3227–3234.

16. van Dam, D.; Abujetas, D.R.; Paniagua-Dominguez, R.; Sánchez-Gil, J.A.; Bakkers, E.P.; Haverkort, J.E.; Gómez Rivas, J. Directional and polarized emission from nanowire arrays. *Nano Lett.* **2015**, *15*, 4557–4563.
17. Anttu, N. Modifying the emission of light from a semiconductor nanowire array. *J. Appl. Phys.* **2016**, *120*, 043108.
18. Kivisaari, P.; Chen, Y.; Anttu, N. Emission enhancement, light extraction and carrier dynamics in InGaAs/GaAs nanowire arrays. *Nano Futures* **2018**, *2*, 015001.
19. Friedler, I.; Sauvan, C.; Hugonin, J.; Lalanne, P.; Claudon, J.; Gérard, J. Solid-state single photon sources: The nanowire antenna. *Opt. Express* **2009**, *17*, 2095–2110.
20. Bleuse, J.; Claudon, J.; Creasey, M.; Malik, N.S.; Gérard, J.; Maksymov, I.; Hugonin, J.; Lalanne, P. Inhibition, enhancement, and control of spontaneous emission in photonic nanowires. *Phys. Rev. Lett.* **2011**, *106*, 103601.
21. Bulgarini, G.; Reimer, M.E.; Zehender, T.; Hocevar, M.; Bakkers, E.P.; Kouwenhoven, L.P.; Zwiller, V. Spontaneous emission control of single quantum dots in bottom-up nanowire waveguides. *Appl. Phys. Lett.* **2012**, *100*, 121106.
22. Anttu, N. Connection between modeled blackbody radiation and dipole emission in large-area nanostructures. *Opt. Lett.* **2016**, *41*, 1494–1497.
23. Anttu, N.; Xu, H. Efficient light management in vertical nanowire arrays for photovoltaics. *Opt. Express* **2013**, *21*, A558–A575.
24. Anttu, N.; Namazi, K.L.; Wu, P.M.; Yang, P.; Xu, H.; Xu, H.; Håkanson, U. Drastically increased absorption in vertical semiconductor nanowire arrays: A non-absorbing dielectric shell makes the difference. *Nano Res.* **2012**, *5*, 863–874.
25. Ba Hoang, T.; Moses, A.F.; Ahtapodov, L.; Zhou, H.; Dheeraj, D.L.; van Helvoort, A.T.; Fimland, B.; Weman, H. Engineering parallel and perpendicular polarized photoluminescence from a single semiconductor nanowire by crystal phase control. *Nano Lett.* **2010**, *10*, 2927–2933.
26. Yuan, X.; Weyhausen-Brinkmann, F.; Martín-Sánchez, J.; Piredda, G.; Krápek, V.; Huo, Y.; Huang, H.; Schimpf, C.; Schmidt, O.G.; Edlinger, J. Uniaxial stress flips the natural quantization axis of a quantum dot for integrated quantum photonics. *Nat. Commun.* **2018**, *9*, 1–8.
27. Chen, Y.; Kivisaari, P.; Pistol, M.; Anttu, N. Optimization of the short-circuit current in an InP nanowire array solar cell through opto-electronic modeling. *Nanotechnology* **2016**, *27*, 435404.
28. Anttu, N.; Kivisaari, P.; Chen, Y. Tailored emission to boost open-circuit voltage in solar cells. *J. Phys. Commun.* **2019**, *3*, 055009.



© 2020 by the authors. Licensee MDPI, Basel, Switzerland. This article is an open access article distributed under the terms and conditions of the Creative Commons Attribution (CC BY) license (<http://creativecommons.org/licenses/by/4.0/>).